Wave-dependent drag parametrizations and their impact on drag and water levels

A. Sterl

Wave-dependent drag parametrizations and their impact on drag and water levels

Andreas Sterl

Koninklijk Nederlands Meteorologisch Instituut (KNMI)
P.O. Box 201, NL-3730 AE De Bilt, Netherlands
phone: +31-30-2206766; e-mail: sterl@knmi.nl

July 16, 2019

Abstract

In this report two aspects of wave-dependent drag parametrisations are discussed. The first chapter contains a short review of different methods to parametrize the roughness length dependent on wave information. Based on the review it is recommended to use a parametrization based on the wave-induced stress for a planned exploratory investigation of coupled atmosphere-wave effects.

In the second chapter wave information obtained from a wave model run on the North Sea is used to derive wave-dependent fields of roughness lengths and drag coefficients. As expected, the wave-dependence introduces scatter into the relation between wind speed and drag coefficient, which is absent in the non-wave dependent parametrization. However, the scatter is small, and the correlation between drag coefficient and wind speed remains high. Therefore, no large-scale effects on the modelled drag or modelled wave and surge heights are to be expected. At least for the North Sea, coupling effects between waves and atmosphere appear not to be important.

Contents

Samenvatting

Om de uitwisselingsprocessen tussen lucht en water te kunnen modelleren moet de effectieve ruwheid van het wateroppervlak bekend zijn. De ruwheid bepaald de sterkte van de turbulentie in de lucht en daarmee de stress (schuifspanning - het verticaal transport van impuls) die de atmosfeer op het water uitoefent.

De wind heeft de grootste invloed op de ruwheid. Hogere winden veroorzaken meer en hogere golven, die de ruwheid doen toenemen. Echter, niet alle op een bepaalde locatie aanwezige golfcomponenten zijn direct gerelateerd aan de lokale wind. Elders opgewekte golven kunnen als deining grote afstanden afleggen en een grote bijdrage aan het lokale golfveld leveren. Verder hangt de invloed van een gegeven windveld af van de duur die de wind al uit dezelfde richting waait. Daarom is voor een nauwkeurige beschrijving van de ruwheid van het zeeoppervlak ook golfinformatie nodig.

Het eerste hoofdstuk van dit report bevat een korte review van golfafhankelijke ruwheidsparametrisaties. De in de literatuur beschreven bulk parametrisaties modelleren de oppervlakteruwheid meestal als functie van golfleeftijd of golfsteilheid. Deze parametrisaties worden gewoonlijk gevalideerd door ze te vergelijken met de schaarse, want moeilijk uit te voeren, directe metingen van stress. Beide parametrisaties beschrijven de metingen beter dan één die puur op windsnelheid gebaseerd is, maar blijven in sommige situaties tekortschieten.

In numerieke golfmodellen wordt vaak een parametrisatie gebruikt die gebaseerd is op de golfgeïnduceerde stress. Dat is de verticale impulsflux die rechtstreeks de golven in gaat. Terwijl de bulk parametrisaties maar één golfparameter gebruiken (of golfleeftijd, of golfsteilheid), bevat de golf-geïnduceerde stress informatie uit het hele golfspectrum. Deze parametrisatie wordt meestal gevalideerd door gemodelleerde golfhoogtes met door boeien of satellieten (altimeter) gemeten golfhoogtes te vergelijken. Deze vergelijkingen laten zien dat de modellen goed werken, ook al blijft er een random fout bestaan. In principe adviseren we om deze parametrisatie in de geplande koppelingsexperimenten te gebruiken. Echter, het berekenen van het benodigde integraal over het hele spectrum is niet triviaal. Voor en snelle eerste, snelle inschatting van koppelingseffecten stellen we daarom voor om een van de één-parameter bulk formules te gebruiken, en wel die op de golfsteilheid gebaseerde. Deze geeft de beste resultaten voor gemengde (deining + zeegang) golftoestanden, die het meest relevant zijn voor de kustveiligheid in Nederland.

In het tweede hoofdstuk gebruiken we de schuifspanning uit een atmosfeermodel (Harmonie) om een golfmodel (SWAN) aan te drijven. Op de output van dat model passen we de in het eerste hoofdstuk gereviewde parametrisaties toe. We analyseren de zo verkregen nieuwe dragcoefficiënten met die uit Harmonie, en we gebruiken ze om nieuwe schuifspanningsvelden te genereren. Om het effect van de verschillende parametrisaties op een veiligheidsrelevante parameter te onderzoeken, gebruiken we de gemodificeerde stressvelden om een waterstandsmodel van de Noordzee aan te drijven. We vinden alleen een klein effect met veranderingen die 8% of 15 cm niet overstijgen.

Door de opzet van de doorgevoerde experimenten zijn deze resultaten alleen indicatief. We maken 10-daagse simulaties van maar drie stormen, zo dat onze resultaten statistisch niet robuust zijn. Bovendien verwaarlozen we de terugkoppeling tussen de gemodificeerde dragcöefficienten en de windsnelheid. De gevonden veranderingen zijn daarom een bovenlimiet van de veranderingen die in een gekoppelde setting te verwachten vallen. De gevonden kleine veranderingen in gesimuleerde waterstanden zullen dan nog kleiner worden. Koppelingseffecten tussen atmosfeer en golven lijken niet relevant te zijn, tenminste niet voor de Noordzee.

Executive Summary

When modelling air-sea interaction, the effective roughness of the air-water interface has to be known. The roughness determines the degree of turbulence in the air and therefore the stress (vertical momentum transport) that the atmosphere exerts on the ocean.

To first order, the roughness depends on the wind, as higher winds make more and higher waves, and waves act as surface roughness elements. However, not all wave components present at a certain location are directly linked to the wind. Waves generated at a remote location can travel large distances as swell and contribute to the local wave field. Furthermore, the impact of a given wind field on the wave field depends on the duration the wind has been blowing from the same direction. Therefore, wave information is needed to achieve a more accurate description of the surface roughness.

In the first chapter of this report a short review of wave-dependent roughness parametrizations is performed. Bulk parametrizations of surface roughness usually model the roughness as a function of wave age or wave steepness. These parametrizations are usually evaluated against sparse and difficult to perform direct stress measurements. While both choices have their merits, they fail in certain situations.

A parametrization frequently used in numerical wave modelling is based on the wave induced stress. This is the vertical momentum flux that goes directly into the waves. Rather than using one wave parameter (wave age or wave steepness), it uses information from the full spectrum. To evaluate this parametrization, modelled wave heights are compared to wave heights measured by buoys or by satellite altimetry. These assessments show a good performance of the model, although some scatter remains. In principle, we recommend to use this parametrization. However, the calculation of the involved integral over the spectrum is not trivial. For a quick first-order test of coupling effects, we therefore recommend the use of one of the one-parameter bulk formulations, namely the one based on wave steepness. It has shown to perform best in mixed (swell + wind sea) conditions, which are most relevant for coastal safety in the Netherlands.

In the second chapter we use the stress from an atmosphere model (Harmonie) to drive a wave model (SWAN) and apply the parametrizations reviewed in the first chapter to the wave model output. We compare the resulting drag coefficients with those used in the driving model, and we use them to derive modified stresses. To investigate the effect of the different parametrizations on a safety-relevant parameter, we use the modified stress fields to drive a barotropic circulation model of the North Sea. We find only small effects, with changes not exceeding 8% or 15 cm.

Due to the set-up of the experiments performed these results are only tentative. As we only analyse three storms, using ten-day simulations, our results are not statistically robust. Furthermore, we neglect the (negative) feedback between the modified drag coefficients and the wind speed. The changes we observe are therefore an upper bound for the changes that are to be expected in a coupled setting. Taking coupling effects into account will reduce the small effect on water level even more. At least for the North Sea, coupling effects between waves and atmosphere appear not to be important.

Chapter 1

A short review of roughness-length parametrizations

Abstract

When modelling air-sea interaction, the effective roughness of the air-water interface has to be known. The roughness determines the degree of turbulence in the air and therefore the stress (vertical momentum transport) that the atmosphere exerts on the ocean. This chapter contains a short review of different methods to parametrize the roughness length dependent on wave information. Based on the review it is recommended to use a parametrization based on the wave-induced stress for a planned exploratory investigation of coupled atmosphere-wave effects. This parametrization uses information from the full spectrum rather than only from its peak. It is used widely in numerical modelling and operationally at ECMWF and has proven to yield good results in terms of wave height. However, as its implementation is somewhat complicated, the use of a simpler parametrization based on wave steepness is recommended for a quick test of the impact on coupled effects.

1.1 Motivation

When modelling air-sea interaction, the effective roughness of the air-water interface has to be known. The roughness determines the degree of turbulence in the air and therefore the stress (vertical momentum transport) that the atmosphere exerts on the ocean.

To first order, the roughness depends on the wind, as higher winds make more and higher waves, and waves act as surface roughness elements. However, not all wave components present at a certain location are directly linked to the wind (swell), and the impact of a given wind field on the wave field depends on the period of time the wind is acting. Therefore, wave information is needed to achieve a more accurate description of the surface roughness. We here perform a short review of wave-dependent roughness parametrizations.

The purpose of this review is to identify a parametrization that allows to check the first order effects of feedback from the waves to the atmospheric flow. The purpose is not to find the ultimate description of wave-atmosphere interaction. Presently, we simply do not have enough knowledge to fully describe this interactions. As Cavaleri et al. (2018) put it, "we still have a long way to go before having a good physical description of the interplay between wind and waves".

1.2 Theoretical background

1.2.1 Atmospheric stress

The stress τ_{atm} exerted by the wind on the ocean is usually parametrized as

$$\tau_{\mathrm{atm}} = \rho_a\, u_*^2 = \rho_a\, C_{D,z}\, U_z^2, \tag{1.1}$$

where ρ_a is the density of air, u_* the *friction velocity*, U_z the wind speed at a height z above the sea surface, and $C_{D,z}$ the corresponding *drag coefficient*. Usually, $z = 10$ m is used as the reference height, and this value is used here. For convenience, we will use the abbreviation C_D for $C_{D,10}$.

Over a flat surface and under neutral atmospheric stratification, the wind profile is logarithmic (see Tennekes, 1973),

$$U(z) = \frac{u_*}{\kappa} \ln\!\left(\frac{z}{z_0}\right), \tag{1.2}$$

where $\kappa = 0.41$ is the von Kármán constant and z_0 the *roughness length*. Together with (1.1) this gives

$$C_D = \left(\frac{u_*}{U_{10}}\right)^2 = \frac{\kappa^2}{\ln^2\!\left(\frac{10}{z_0}\right)}. \tag{1.3}$$

Over land, the evolution of surface characteristics is slow (e.g., due to plant growth), and for short periods (days) the roughness length is constant in time, while varying in space. However, the roughness of the sea surface depends on the sea state and changes rapidly. The varying roughness length is usually parametrized as

$$z_0 = 0.11\frac{\nu}{u_*} + \alpha\frac{u_*^2}{g}, \tag{1.4}$$

where ν is the kinematic viscosity of air, g the acceleration due to gravity, and α the *Charnock parameter*. The first term in (1.4) describes the effect of viscosity on the roughness and is only relevant at low wind speeds. The second term in (1.4) has been introduced by Charnock (1955) and is meant to describe the effect of the sea state. Usually, the Charnock parameter is treated as a constant. Neglecting variations in air density this implies a one-to-one relation between wind speed and roughness length and, consequently, stress.
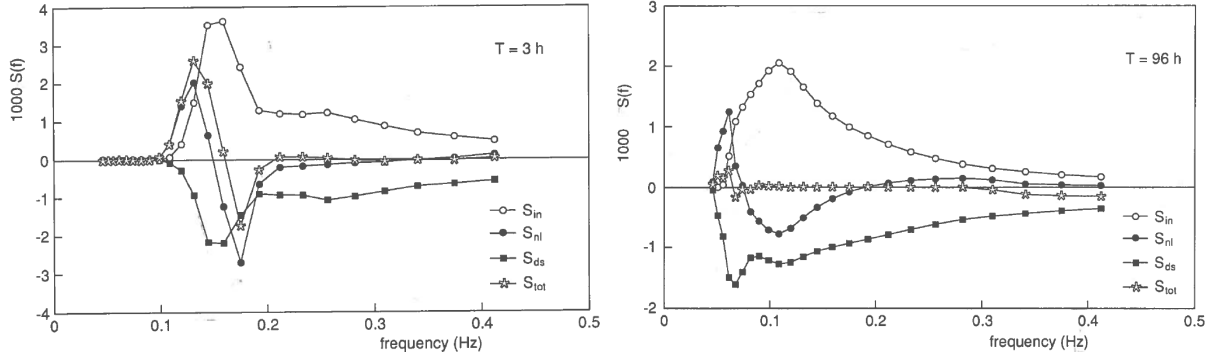
Figure 1.1: The energy balance for (*left*) young duration-limited sea (3 hours after storm onset) and (*right*) old wind sea (96 hours after onset) in deep water ($S_{bot} = 0$). (These are Figs. 3.9 and 3.10 from Komen et al., 1994.)

Equations (1.1), (1.3) and (1.4) describe an implicit relation between the drag coefficient, the friction velocity and the wind speed. In section 1.3 we review different parametrizations of this implicit relation.

1.2.2   Wave stress

In wave modelling, waves are usually described by the *energy density spectrum $E(\vec{x}; \omega, \varphi)$*. For each position $\vec{x}$ it specifies the amount of energy at (angular) frequency ω travelling in direction φ. The development of the energy density spectrum is described by the energy balance equation

$$\frac{\partial E}{\partial t} + \vec{\nabla} \cdot (\vec{c}_g E) = S_{in} + S_{nl} + S_{ds} + S_{bot}. \tag{1.5}$$

The first term on the left describes the change of the energy density E with time, and the second the advection of energy with the group velocity c_g. The terms on the right are the source terms:

S_{in} — energy input from the wind. In the widely used WAM model (Komen et al., 1994) this term is given by

$$S_{in} = \gamma N, \tag{1.6}$$

where $N = E/\sigma$ is the action density, γ is the wave growth factor, and σ the intrinsic frequency (frequency of free travelling surface waves in deep water).

S_{nl} — redistribution of wave energy by non-linear four-wave interaction to higher and lower frequencies. Subsequently, high-frequency waves will break (dissipation, S_{ds}), while low-frequency waves gain energy and grow. Together, these two effects result in a shift of the peak frequency of the energy spectrum,

S_{ds} — loss of wave energy through dissipation (whitecapping),

S_{bot} — loss of wave energy by interaction with the bottom: friction, depth-induced breaking and non-linear three-wave interactions.

The magnitude of the three source terms S_{in}, S_{nl}, S_{ds} and their sum is shown in Fig. 1.1 for young (3 hours after storm onset) and old (96 hours after onset) wind sea. For young sea the wind input is larger than for old sea. Young sea is steeper (rougher) than old sea. In both cases a large part of the wind input is directly lost to the ocean via whitecapping (dissipation). Despite the large loss young waves still gain energy ($S_{tot} > 0$ if integrated over frequency) and grow. For old waves the loss is nearly complete ($S_{tot} \approx 0$), and the waves do not grow any more.

3

The wind input source term S_{in} represents the *energy flux* from the atmosphere to the waves. The corresponding *momentum flux*, i.e., the *wave-induced stress*, is given by (Janssen, 1991)

$$\vec{\tau}_{\mathrm{wav}} = \rho_w\, g \int_0^{2\pi} \int_0^{\infty} \frac{\vec{k}}{\omega} S_{\mathrm{in}}\, d\omega\, d\varphi, \tag{1.7}$$

where $\vec{k}$ is the wave vector and ρ_w the water density. Replacing S_{in} in this equation by S_{ds} or S_{bot} yields expressions for $\vec{\tau}_{\mathrm{ds}}$ and $\vec{\tau}_{\mathrm{bot}}$, which describe the momentum *lost* by the waves due to dissipation and bottom effects, respectively.

1.3 Overview of parametrizations

We here give a short assessment of drag parametrizations. As we are mainly interested in situations with high wind speeds, viscosity effects as described by the first term in (1.4) are neglected.

1.3.1 Parametrizations as a function of wind speed

Often the Charnock parameter α is assumed to be constant. In this case the implicit relation given by (1.1), (1.3) and (1.4) can be well approximated by a linear relation between the drag coefficient and the wind speed,

$$C_D = a + b\, U_{10}, \tag{1.8}$$

where $a \approx 0.5$ and $b \approx 0.065~(\mathrm{m/s})^{-1}$ are typical values. Drag measurements can be well described by such a linear relation, albeit with large scatter.

At very high wind speeds ($U_{10} \gtrsim 30$ m/s) the wind tears droplets away from the breaking waves, forming a layer of spray above the wave crests. This layer effectively decouples the atmosphere from the water surface, and the air flow experiences less drag. As a consequence, the drag coefficient grows slower than linear with wind speed, and eventually even declines (saturation). A parametrization with a quadratic dependence on wind speed mimicking this behaviour (see Zijlema et al., 2012) is available in SWAN. More details on drag parametrizations as a function of wind speed can be found in Sterl (2017).

1.3.2 Parametrizations including wave parameters

The surface roughness is not completely determined by the local wind. Waves that were generated far away can enter a region as swell (see Sect. 1.3.3), without any relation to the local wind field, and the characteristics of locally generated waves depend, at the same wind speed, on the time the wind has been blowing in the same direction. Young waves, waves that are generated at the beginning of a storm, are steeper (rougher) than old waves (see Sect. 1.2.2). It is therefore natural to add wave information to the parametrization of the roughness length. This is usually done by making the Charnock parameter α dependent on wave information. Parameters used to convey the wave information are the wave steepness s and the wave age ξ.

The wave steepness is defined as the ratio of the significant wave height H_s to the wave length L_p at the peak of the wave spectrum,

$$s = H_s/L_p. \tag{1.9}$$

Taylor and Yelland (2001) parametrize the roughness length as a function of s as

$$\frac{z_0}{H_s} = 1200\, s^{4.5}. \tag{1.10}$$

The wave age is a measure of the speed of the dominant waves to a speed characterising the local wind. It is either defined as

$$\xi_* = c_p/u_*, \quad \text{or as} \quad \xi = c_p/U_{10}, \quad (1.11)$$

where c_p is the phase speed of the waves at the peak of the wave energy spectrum. During a storm, the peak of the spectrum shifts from high to low frequencies (see also the wind-input term S_{in} in Fig. 1.1). According to the dispersion relation for deep-water waves ($c = g/\omega$), low-frequency waves are faster than high-frequency ones. Thus at the beginning of a storm, c_p and wave age are small, and the waves are young. The wind blows faster than the dominant waves travel. The waves are driven by the wind, i.e., momentum is extracted from the atmosphere and transferred to the growing waves. In the case of old waves (high wave age), the dominant waves travel faster than the wind, and the transfer of momentum from the atmosphere to the waves is small. The Charnock parameter is usually parametrized as some power of the inverse wave age, making the surface rougher for young waves. For instance, Drennan et al. (2005) suggest

$$\frac{z_0}{H_s} = 3.35\,\xi_*^{-3.4}. \quad (1.12)$$

A variation was suggested by Oost et al. (2002), who used $z = L_p$, the length of the waves at the spectral peak, as the reference height. This height is related to the wave field and thus has a physical meaning, while the usually chosen height of 10 m is rather arbitrary. He finds

$$\frac{z_0}{L_p} = \frac{50}{2\pi}\xi_*^{-4.5}, \quad (1.13)$$

where, based on a Pierson-Moskowitz spectrum (e.g., Stewart 2008, Sect. 16.4), L_p can be related to $U_{19.5}$, the wind at a height of 19.5 m, as

$$L_p = \frac{g}{2\pi}\,(0.729\,U_{19.5})^2. \quad (1.14)$$

This parametrization is available in Harmonie through the SURFEX surface module (Le Moigne, 2018). Note that Le Moigne (2018) do not specify the height of U in their equation (2.40), but according to the numerical values they provide, U must be given at the height of 19.5 m. The SURFEX code should be checked whether (1.14) is implemented correctly.

Note that in all parametrizations listed above the viscous term ($0.11\frac{\nu}{u_*}$; see (1.4)) has to be added to account for low-wind conditions.

1.3.3 Impact of swell

After being generated, waves can travel long distances without much dissipation. These waves are called swell and are unrelated to the local wind. There can be waves without wind. If the swell is strong enough it can drive the atmosphere, i.e., the momentum transport is reversed (Grachev and Fairall, 2001).

Investigating a large data set from the Baltic Sea, Smedman et al. (2003) find that a logarithmic wind profile only exists over young waves. As they travel slower than the wind speed, the atmosphere "sees" them as quasi-stationary roughness elements, giving rise to the same interaction processes as over land. In the presence of swell, however, this similarity breaks down and deviations from the logarithmic wind profile occur, confirming earlier findings of Drennan et al. (1999). While for young waves the roughness length can be parametrized with the wave age alone, Smedman et al. (2003) find that a second parameter is needed for swell cases, namely the ratio between the energy of the relatively long and the relatively short waves, respectively.

The impact of swell on the drag coefficient is further investigated by Högström et al. (2015). Removing the swell impact from their data (using a method from Rieder and Smith, 1998), they

find that the residual "pure wind sea part" of the drag can be described by an equation of the form (1.8), but that in swell-dominated situations the drag coefficient becomes dependent on the swell factor $H_{sd} f_n$ (H_{sd}: significant height of swell, f_n: frequency of the dominant swell), leading to C_D values that can be several times larger than those for the pure wind sea case (1.8). Note, however, that Högström et al. (2015) only consider moderate wind speeds (below 10 /ms).

1.3.4 Parametrization using full spectral information

In the parametrizations described above, only a limited part of the information available from the wave field is used. It is condensed into one parameter characterizing the peak of the spectrum (L_p or c_p). Janssen (1989, 1991) (see also Komen et al., 1994) has developed a formula in which the full spectral information of the wave field is used. Assuming a logarithmic wind profile and a constant stress layer close to the surface, he expresses the Charnock parameter as a function of the wave induced stress (1.7),

$$\alpha = \frac{\hat{\alpha}}{\sqrt{1 - \tau_{\text{wav}}/\tau_{\text{atm}}}}, \qquad \hat{\alpha} = 0.006, \qquad (1.15)$$

where τ_{wav} and τ_{atm} are the moduli of the respective stresses. Because of (1.6) and (1.7), the whole spectrum is involved in the calculation of the Charnock parameter according to (1.15). This parametrization is used as the default in WAM (Komen et al., 1994) and is optionally available in SWAN (SWAN, 2018) and in WWW3 (Tolman, 2009).

Note that to calculate τ_{wav}, the integral in (1.7) has to be taken over all frequencies, including the high-frequency part which is usually not resolved by a wave model. Originally, Janssen (1991) assumed a f^{-4} relation for that part, but the current implementation in WAM as used operationally at ECMWF employs a f^{-5} relation because it is in better agreement with observations (ECMWF, 2017). The choice of the form of the tail is reported not to impact the results of the wave model, except for the wave induced stress. Furthermore, they use a cut-off frequency (the frequency at which the unresolved part is supposed to start) that is dependent on local conditions, namely the mean frequency of the local wind sea (ECMWF, 2017). The use of a dynamic cut-off makes the implementation of parametrization (1.15) less straightforward than the simple one-parameter ones discussed in Sect. 1.3.2.

1.4 Discussion

The bulk parametrizations (α constant, steepness dependent, or wave age dependent) have been widely compared to observational estimates. In general, the two wave-dependent parametrizations score better, but they are not able to describe the stress in all situations. Bonekamp et al. (2002) compare bulk parametrizations with the shipboard measurements of Yelland and Taylor (1996). They conclude that

> [...] all bulk parametrizations score low on goodness-of-fit test. The lowest scores are obtained for the constant Charnock parameter case, whereas the highest scores are obtained for a wave-age-dependent parametrization.

Drennan et al. (2005) test the steepness parametrization (1.10) and the wave-age dependent parametrization (1.12) against eight sets of measurements representing a wide range of conditions. They find that

> [in] conditions with a dominant wind-sea component, both scalings were found to yield improved estimates when compared with a standard bulk formulation [constant α; A.S.]. In general mixed sea conditions, the steepness formulation was preferred over both bulk and wave-age scalings, while for underdeveloped "young" wind sea,

the wave-age formulation yields the best results. Neither sea-state model was seen to perform well in swell-dominated conditions where the steepness was small, but the steepness model did better than the wave-age model for swell-dominated conditions where the steepness exceeded a certain threshold.

That failure of the parametrizations in swell-dominated situations confirms the findings of Smedman et al. (2003) (see Sect. 1.3.3).

Note that all comparisons between observational estimates of roughness or stress and the corresponding model results exhibit high scatter. On the one hand this is probably due to difficulties in measuring these quantities, but it also shows that the surface roughness depends on more than one or two parameters.

A limitation of the evaluation of Drennan et al. (2005) is that stress measurements over sea are only available for moderate wind speeds ($U_{10} \lesssim 25$ m/s). Therefore, new physical effects that occur a high wind speeds are not accounted for. Especially, the impact of drag saturation (see Sect 1.3.1) is not taken into account.

Zhao and Li (2019) analyse combined laboratory and *in situ* measurements of stress. For low to moderate wind speeds ($U_{10} < 25$ m/s), they find a high correlation between wave age and wave steepness. This relation can be obtained theoretically from the dispersion relation of surface waves in deep water. So in this wind speed range, the two parameters could be used interchangeably. For higher wind speeds, the wave steepness stops increasing due to wave breaking, but wave age continues to decrease with wind speed. Assuming a maximum value of 1/7 for wave steepness (Stokes waves), they arrive at

$$z_0 = \left\{ \begin{array}{l} 3.5153 \times 10^{-5} \times \xi^{-0.42}\, U_{10}^2/g \\ 2.1583 \times 10^{-4} \times \xi^{1.56}\, U_{10}^2/g \end{array} \right. \quad \text{for} \quad \begin{array}{l} \beta > 0.4 \\ \beta \leq 0.4 \end{array} . \tag{1.16}$$

This equation can be used if no steepness information is available, and the drag coefficient can be determined from (1.2). If steepness information is available, Zhao and Li (2019) apply the 3/2 power law of Toba (1972) and find that the drag coefficient can be expressed as

$$C_D = 3.0196 \times 10^3\, s^4\, \xi^2. \tag{1.17}$$

Applying this equation to laboratory data, Zhao and Li (2019) find that C_D decreases for wind speeds exceeding 25 m/s. Note that the saturation of the drag coefficient at high wind speed here arises just from a combination of geometry (steepness) and wind strength (wave age), without any need to invoke spray layers (see the discussion in Sterl (2017)).

Shimura et al. (2017) use the three roughness parametrizations (1.8), (1.10) and (1.12) in runs with a global atmosphere model. Comparing the resulting wind fields, they find that wind speeds in the tropics are better simulated with a wave-dependent roughness length than they are for the constant Charnock parameter case, but that they are deteriorated in the mid-to-high latitudes. They ascribe the better performance of the wave-dependent parametrizations in the tropics to the fact that the tropics are swell-dominated. The waves are smooth, and using the wave-dependent parametrizations leads to a smaller Charnock parameter and thus higher winds, which brings their modelled winds closer to observational estimates. Likewise, they attribute the deterioration in mid-to-high latitudes to the fact that "the global ocean displays a wide range of climatology and wave characteristics", with no universal relation between wind, waves, and roughness. Note that these results are somewhat at odds with those of Drennan et al. (2005) cited above.

The Integrated Forecast System (IFS) of ECMWF uses the wave induced stress parametrization (1.15) to calculate the Charnock parameter. Therefore, IFS consists of a coupled atmosphere-wave model. A typical comparison between observed and modelled significant wave heights is shown in Fig. 1.2. The correspondence between observed and modelled wave heights is large for all wave heights, suggesting that parametrization (1.15) works well. Unfortunately, a direct
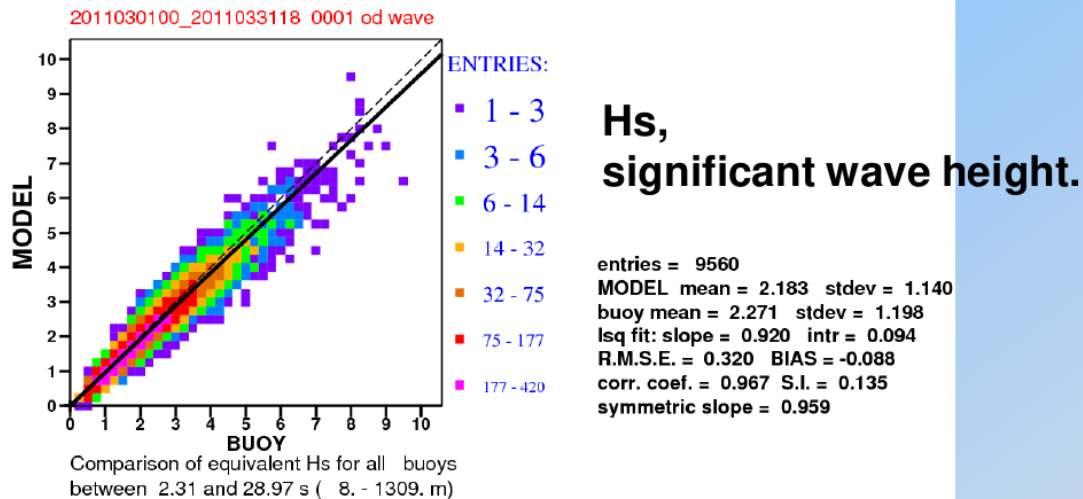
Figure 1.2: Scatter plot of observed (buoys) and modelled significant wave heights for March 2011. Modelling has been done using the ECMWF forecast system. The figure is taken from Bidlot (2012).

comparison of measured and modelled roughness lengths or stresses is not possible as such measurements only exist from dedicated measurement campaigns, i.e., for short periods of time and at a very limited number of points in space.

Pineau-Guillon et al. (2018) use the ECMWF coupled system to perform simulations of some mid-latitude storms. They find the model to underestimate the wind and conclude that the modelled roughness is too high. So the good correspondence between modelled and observed wave heights as displayed in Fig. 1.2 is probably the result of compensating errors, too low winds combined with too high drag resulting in correct wave heights. Another interesting result of Pineau-Guillon et al. (2018) is that the drag coefficient saturates at about 25 m/s. This occurs despite the model not including any parametrization of a spray layer that decouples the air flow from the direct influence of the waves, the explanation that is usually given for the observed drag saturation (Sterl, 2017).

In addition to the wave-induced stress parametrization (1.15), Pineau-Guillon et al. (2018) also employ several alternative parametrizations, among which the wave-age dependent one of Oost et al. (2002) (1.12). They find the latter to produce unrealistically high values of the Charnock parameter and the associated drag coefficient at wind speeds above 25 m/s.

1.5   Summary and Conclusions

Different parametrizations of the roughness length (or, equivalently, the Charnock parameter) have been reviewed. Parameterizations including *one* wave parameter (steepness or wave age) clearly perform better than does the constant-Charnock parametrization, but are still not able to cover all wave conditions. A coupled wave-atmosphere model based on the wave-induced stress that uses information from the *full* wave spectrum is able to produce wave heights that compare well with observations over a wide range of wave heights.

All parametrizations are based on the assumption of Monin-Obukhov similarity. As this assumption may not be valid in the presence of strong swell and weak winds, the parametrizations may fail under such conditions. However, low-wind conditions are of little relevance for coastal safety. Therefore, this possible failure of the parametrizations can be ignored for this purpose.

None of the wave-dependent parametrizations accounts for the drag-saturation effect. Due to the physics involved (tearing-off of droplets from breaking waves) this effect is probably predominantly a wind effect and independent of the wave field. Interestingly, the parametrization

based on the induced stress shows some saturation despite the fact that it is not explicitly modelled. It is as yet unclear how the drag-saturation effect has to be included in wave-dependent drag parametrizations.

For a systematic investigation of wave-atmosphere coupling effects in the North Sea the parametrization based on the wave-induced stress (1.15) should be used as it has proven to yield good results for a wide range of wave heights, although it might overestimate the drag at high wind speeds. However, its implementation is somewhat complicated (see Sect. 1.3.4), and the impact of the assumed form of the high-frequency tail of the wave spectrum in calculating the wave-induced stress has to be better understood before applying this parametrization.

For a quick testing of coupling effects it is therefore recommended to use the steepness formulation (1.10). It is preferred above the wave-age dependent formulation (1.12) because it performs better in general mixed-sea conditions, which are most relevant for coastal safety along the Dutch coast. Furthermore, at high wind speeds the wave-age dependent formulation produces unrealistically high values for the Charnock parameter.

Chapter 2

Wave-based drag coefficients from SWAN

Abstract

From 2400 years of data produced by the EC-Earth climate model, the strongest storms occurring in the North Sea have been downscaled with Harmonie, using different drag parametrizations. The stress obtained from these Harmonie runs has been used by Deltares to force SWAN. The SWAN output is used to generate wave-dependent roughness estimates. A comparison is done between these estimates and those of the parametrizations used in the Harmonie runs. The aim is to conclude whether a wave-dependent roughness estimate, together with a two-way coupling between Harmonie and SWAN, has the potential to significantly alter the model outputs. As to be expected, adding a wave-dependence to the drag parametrization increases the spread of the drag parameter for a fixed wind speed. However, the increase in spread is small, and the correlation between modelled drag coefficient and wind speed remains high, leading to the conclusion that a parameterization just in terms of wind speed suffices for the North Sea.

2.1 Introduction

In Chapter 1 we have discussed wave-dependent roughness parametrizations. In this chapter we investigate whether the introduction of wave-dependence has the potential to significantly alter the modelled stress field in the North Sea, and consequently modelled wave and surge heights.

To do so, we use the stress output from a high-resolution atmosphere model to drive a wave model. The output of the wave model is used to derive wave-dependent drag coefficients, which are compared with the non-wave dependent ones used in the driving atmosphere model. We investigate whether the differences affect the correlation between drag coefficient and wind speed in a way (temporal and spatial extent) that it is able to significantly influence the modelled stress field and, consequently, wave height and surge height.

The atmosphere model used is Harmonie (Bengtsson et al., 2017), which is operationally used at KNMI. The domain covers the North Sea and parts of the north-east Atlantic. The northern and western boundaries are roughly at 64°N and 15°W, respectively, and the horizontal grid resolution is 2.5 km. At the lateral boundaries, Harmonie is forced by fields from the EC-Earth climate model (Hazeleger et al., 2012).

The wave runs were performed by Deltares using the SWAN (SWAN, 2018) model. It is run on a domain similar to the Harmonie domain, with a horizontal resolution of 0.05° ($\approx$ 5 km). The maps in this report show the whole SWAN domain. The Harmonie output has been regridded to the SWAN grid, and all analyses are performed on the SWAN grid. More details about the SWAN runs can be found in appendix 2.A.

2.2 The runs

The basis of the experiments are more than 2400 years of output from the EC-Earth climate model (Van der Wiel et al., 2019), from which three major storms have been selected according to the following criteria,

A the storm resulting in the highest surge in Hoek van Holland,

B the storm with the highest wind speed occurring over the North Sea,

C the storm with the highest wind speed over Lake IJssel.

These three storms haven been downscaled by Harmonie (Bengtsson et al., 2017) using three different parametrizations of the drag coefficient,

1 ECUME, the default parametrization used operationally at KNMI,

2 a Charnock relation (eq. (1.4)) with a Charnock constant $\alpha = 0.015$,

3 a Charnock relation with $\alpha = 0.032$.

The resulting drag coefficients C_D as a function of wind speed U_{10} are depicted in Fig. 2.1. We will refer to the different combinations of storm and parametrization by the respective letter-number combination.

Harmonie uses the SURFEX (Le Moigne, 2018) scheme to calculate the interaction between the atmosphere and the surface. Within SURFEX, each grid box is composed of four surface types (*tiles*), two of which deal with water, *lake* and *sea*. For surfaces classified as *lake* (real lakes, but also large parts of the Wadden Sea), the surface roughness is determined from a Charnock relation (1.4) with $\alpha = 0.015$. For surfaces classified as *sea* several parametrizations are available, the standard one being ECUME (Le Moigne, 2018). When ECUME is used for *sea* tiles, the Charnock parameter is set to $\alpha = 0.02$ for the *lake* tiles.

The stress fields from the downscaled runs have then been used by Deltares to force their wave model SWAN (SWAN, 2018). Details about the forcing can be found in appendix 2.A.
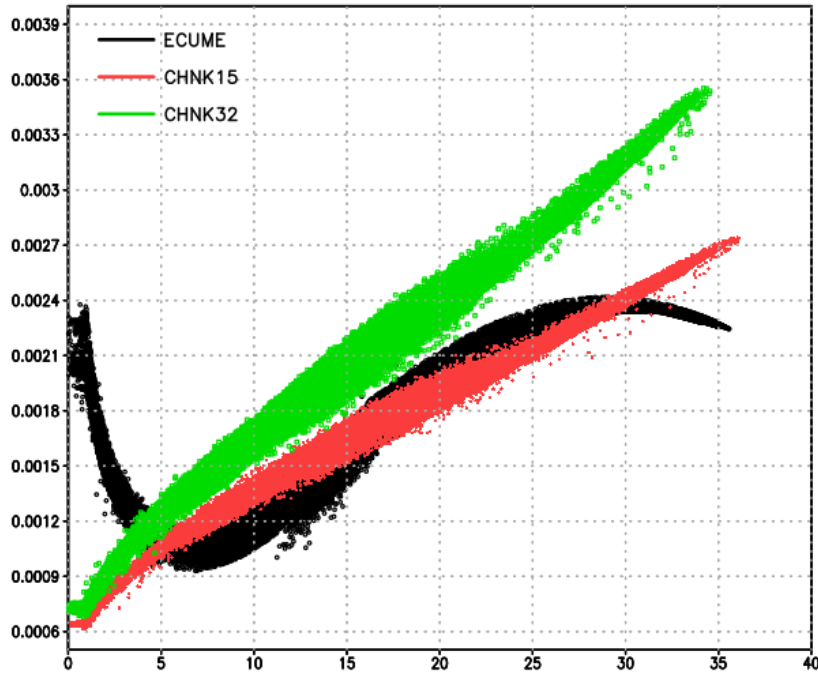
Figure 2.1: Scatter plot of drag coefficient C_D versus wind speed U_{10} from storm B for the three parametrizations employed.

The SWAN output does not contain the parameters wave age and wave steepness that are needed in the wave-dependent roughness length parametrizations directly, but they can be calculated from the available output. We refer to the different parametrizations (eqs. 1.10, 1.12, 1.13, 1.16, and (1.17) as steep, ustar, oost, zhao36, and zhao39, respectively (36 and 39 are the corresponding equation numbers in Zhao and Li (2019)).

Wave steepness can simply be calculated as $s_p = H_s/L_p$, where H_s and L_p are significant wave height and peak wavelength, respectively, and both variables are present in the SWAN output. The wave age $\xi_* = c_p/u_*$ needs input from SWAN (c_p) and from Harmonie (u_*). As the Harmonie output contains the drag coefficient and the wind components, the friction velocity can be calculated from $u_* = \sqrt{C_D}\,U_{h,10}$, where $U_{h,10}$ is the wind speed at 10-m height, calculated from the wind components. The SWAN output does not contain the peak phase speed (c_p). However, it can be calculated as $c_p = \frac{g}{2\pi}T_p$, where T_p is the peak period. This formula for c_p is based on the deep-water dispersion relation for surface gravity waves. As the North Sea can be regarded as shallow for the most relevant waves, one can also calculate a peak phase speed based on the shallow-water dispersion relation as $c_{p1} = L_p/T_p$. It turns out that both choices result in similar estimates of the drag coefficient (not shown). Therefore, only results based on c_p are considered here.

2.3 Wave-dependent drag coefficients

2.3.1 Spatial comparison

The drag coefficients according to different parametrizations are displayed in Fig. 2.2 for one particular time step near the maximum of the storm in run C2 ($\alpha = 0.015$). In this figure,
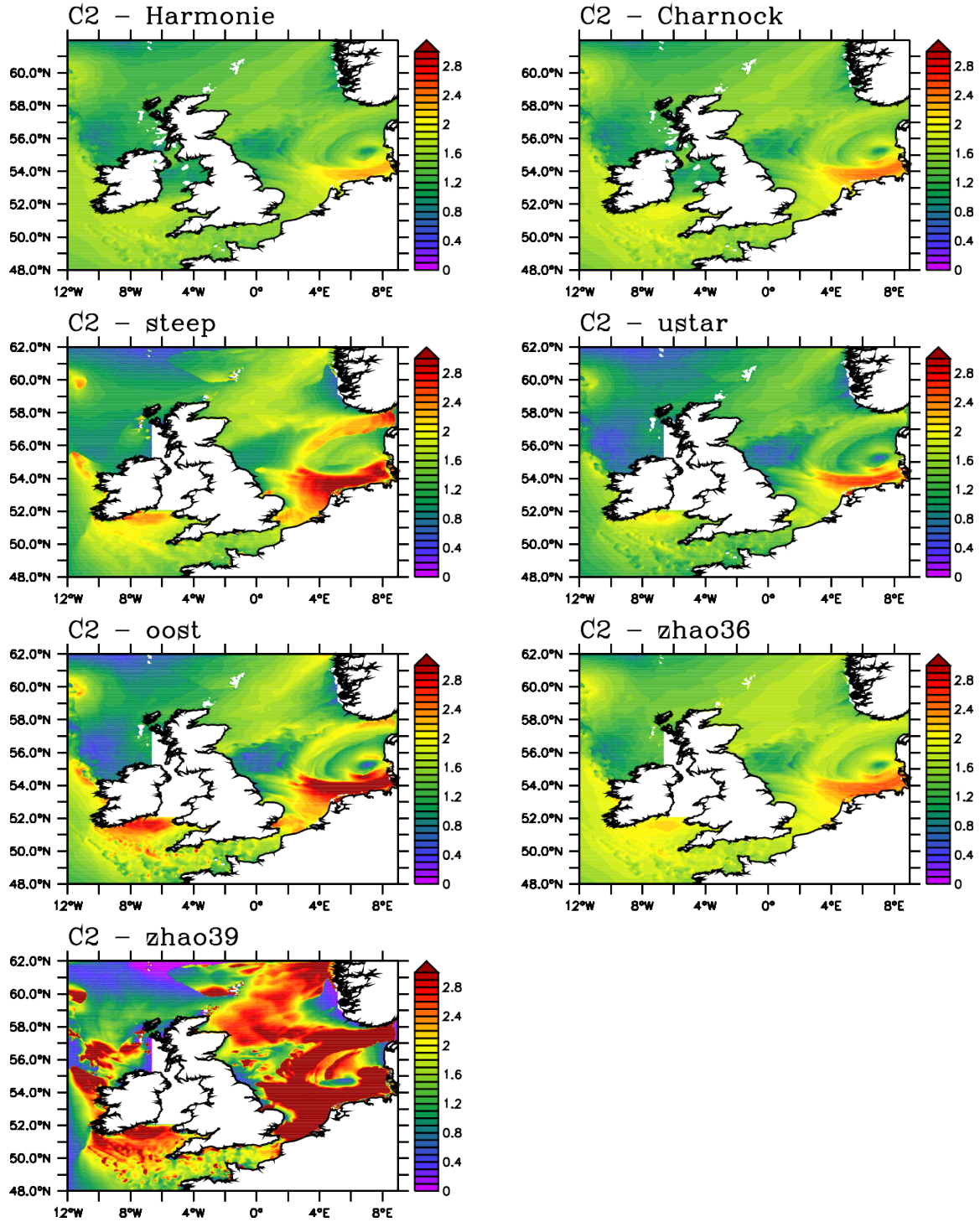
Figure 2.2: Drag coefficients ($\times 10^3$) according to different drag parametrizations as indicated for one particular time step near the maximum of the storm in run C2 ($\alpha = 0.015$). "Harmonie" (upper left) refers to the direct model output, while for "Charnock" (upper right) the drag coefficient has been recalculated using eq. (1.4).
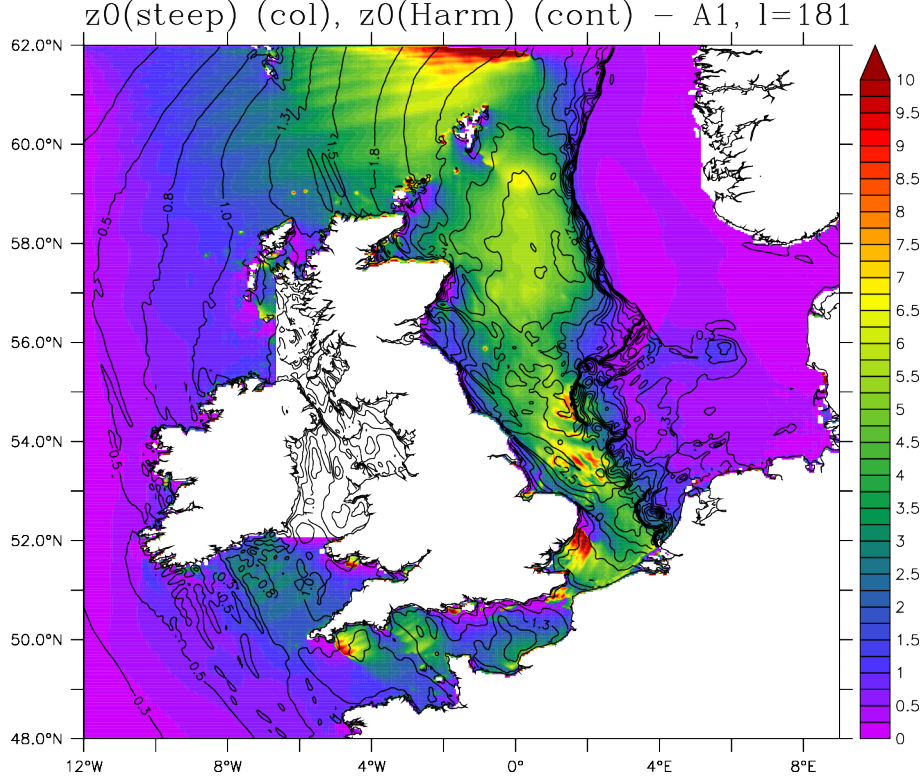
Figure 2.3: Roughness lengths ($\times 10^3$) z_0^{steep} (colours) and z_0^{harm} (contours) for run A1 at one particular time step. Note the distinct north-south structure north of Scotland in z_0^{steep} that is not present in z_0^{harm}. Similar structures are found south of Ireland and Cornwall.

"Harmonie" refers to the direct model output, and "Charnock" (upper right) to the application of eq. (1.4) with a friction velocity determined as $u_* = \sqrt{C_D}\, U_{h,10}$. Unexpectedly, the two drag coefficients differ. The reason is unclear, but there seems to be some inconsistency in the Harmonie output. Calculating drag coefficients from eq. (1.3) using the roughness from the Harmonie output does not reproduce the drag coefficients from the Harmonie output, but yields values that are close to C_D^{charn}.

The spatial patterns of the different drag coefficients are very similar, but the wave-dependent parametrizations result in a larger spatial variation. Wave-dependent drag coefficients are higher near the centre of the storm (near the southern coast) and lower far away from the storm (e.g., east of northern England). Additionally, the steepness-based parametrization leads to a smoothed drag field (less structure). For instance, the "eye" in the centre of the storm is less pronounced than in the other parametrizations. The zhao36 parametrization results in a much smoother field than the other parametrizations, while zhao39 exhibits the largest spatial variation with unrealistically high values ($> 3 \cdot 10^{-3}$) in large areas. We therefore do not consider this parametrizations in the following. It should be noted that increasing the exponent for wave steepness in eq. (1.17) to somewhere between 4.2 and 4.3 results in more realistic values for C_D (not shown). More research is needed to pinpoint the reasons for the unrealistically large drag coefficients resulting from (1.17).

The wave-dependent parametrizations sometimes give rise to some distinct wave-like patterns that are not present in the Harmonie parametrization. For the wave-steepness based parametrization an example is shown in Fig. 2.3, where such a pattern is found around the Shetland Islands. Presumably this wave-like pattern results from the diffraction of swell when passing the islands. Similar patterns are found south of Ireland and Cornwall. The ustar and oost parametrizations show similar, but less vigorous, wave-like structures.

14

2.3.2 Drag relations

Fig. 2.4 shows how the wave-dependence changes the drag coefficient. It contains scatter plots of the drag coefficients according to the different parametrizations against the wave-independent ones produced by Harmonie. In this figure a run with ECUME parametrization is used, but the runs with a Charnock parametrization give similar plots.

All wave-dependent parametrizations result in a large scatter, indicating that taking the wave field into account can modify the drag substantially. Wave-dependence can both increase or decrease the drag coefficient. The smallest change is found for zhao36. This parametrizations mainly reproduces the Charnock one. Its 95% interval is a bit wider than the Charnock one, but only a few values are higher by more than a few percent. They are caused by young waves. In the case of ustar the bulk of the values (median) follows those from ECUME well, while for steep and oost the median increases faster than the one-to-one line. Wave effects systematically increase the drag coefficients for these parametrizations. The distributions are rather symmetric around the median, with ustar skewing to positive deviations at high values of C_D, while steep seems to be negatively skewed everywhere. The largest scatter occurs in steep with the width of the 95%-interval exceeding $1 \ cdot 10^{-3}$, or $\pm 50\%$, at $C_D = 2 \cdot 10^{-3}$. The smallest scatter is found for zhao39.

2.3.3 Relation between C_D and U_{10}

Figures 2.5 and 2.6 display the density of the $C_D(U_{10})$ relations for several drag parametrizations and for all three parametrizations used in the Harmonie runs. The line according to the Wu (1982) parametrization (i.e., (1.8) with $a = 0.8$ and $b = 0.65$, valid for $U_{10} > 6$ m/s) is added as a reference. It represents a good approximation of the ECUME and $\alpha = 0.015$ cases.

The $C_D(U_{10})$ relations resulting from the Harmonie output (upper left panels), as well as those resulting from the Charnock relation (upper right panels) clearly differ between the three runs. For A1 the Harmonie relation curls around the Wu-line, for A2 it lies completely below, and for A3 completely above that line. Contrary to this, the $C_D(U_{10})$ relations for the three wave-dependent parametrizations look very much the same for all Harmonie runs. The reason is that the wave fields do not differ much between the runs, which in turn is due to the driving stress fields not differing much (see also Sect. 2.3.4). Except for small areas, stress and significant wave height differ by less than 12% between runs A2 and A3 when averaged over the total length of the run. The wave-dependent drag coefficients depend on the spectral peak, which is relatively insensitive to small changes in the driving stress field. Therefore, differences in wave steepness and wave age are less than 6%. This translates into differences of less than 2% for the wave-age dependent drag coefficient, and of less than 8% for the steepness-based one.

Figures 2.5 and 2.6 show that except for zhao36 all wave-dependent parametrizations lead to steeper $C_D(U_{10})$ relations than the Wu parametrization, or, by inference, the ECUME and $\alpha = 0.015$ cases, and that they introduce a lot of scatter. Note that the scatter in the Harmonie case (upper left panels) is due to stability effects, not wave effects. The lowest scatter is found for zhao36, and the bulk of the values closely follows the Wu-line. For ustar and oost the scatter increases with wind speed and is positively skewed at high wind speed. For steep the scatter is high everywhere and positively (negatively) skewed at low (high) wind speeds. At a wind speed of 20 m/s, where ECUME gives $C_D = 2 \cdot 10^{-3}$, the width of the 95% interval exceeds $1 \cdot 10^{-3}$, equivalent to $\pm 50\%$.

Despite the scatter, the correlation between wind speed and drag coefficients is high in all cases (Figure 2.7). The low correlation for ECUME (panel a) is due to the behaviour of the drag coefficient at low wind speeds (see Figure 2.5). Indeed, when the calculation is repeated for $U_{10} > 6$ m/s only, the correlation is high everywhere (panel f). In fact, it is higher than those for the other parametrizations, which even become a bit lower (compare panels b-d with g-i).
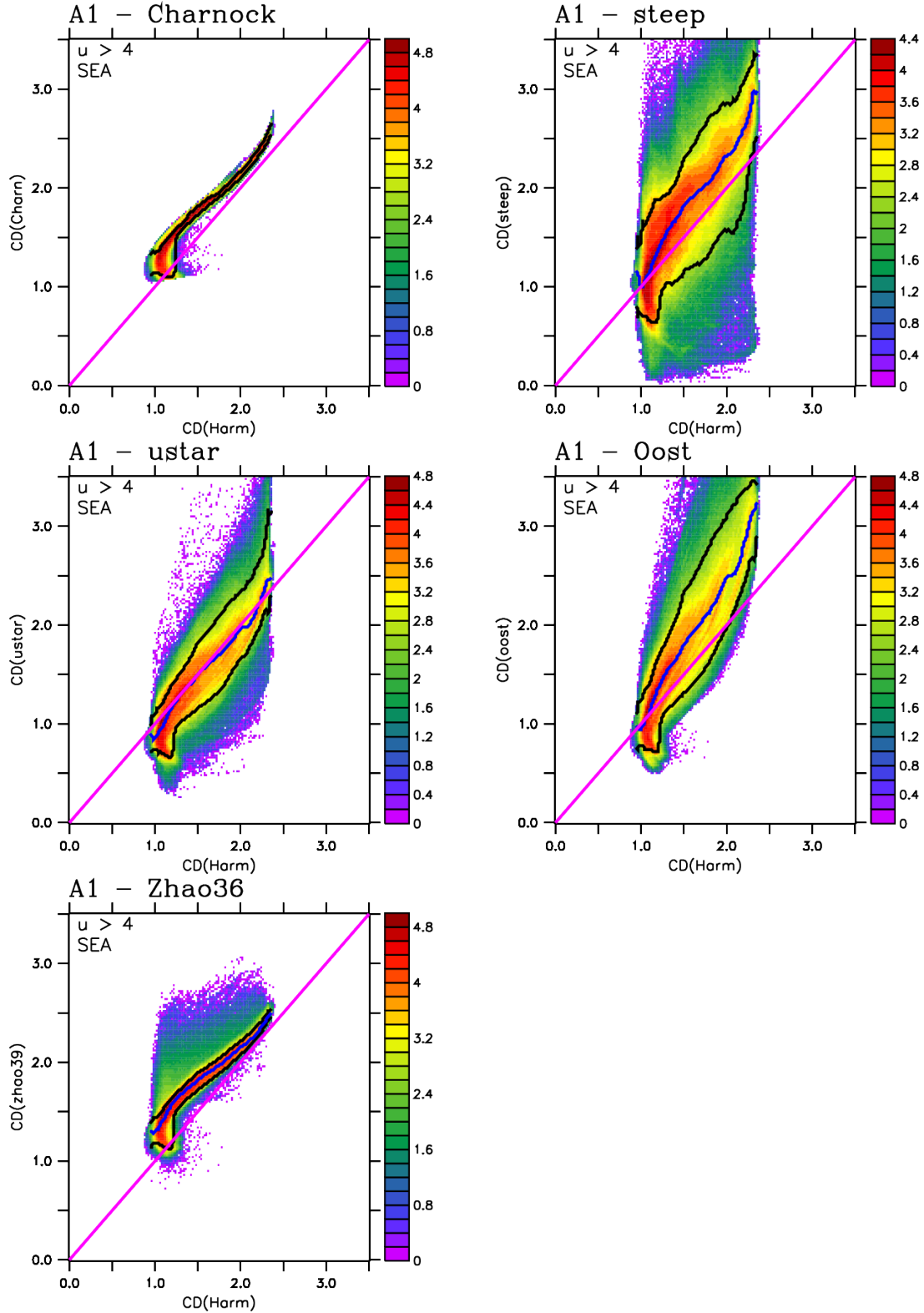
Figure 2.4: Scatter plots (logarithm of the density) of different drag coefficients ($10^3 \times C_D$) against those from run A1 (Harmonie with ECUME). Added as a magenta line is the one-to-one relation. The black contour denotes the 95% interval for each value of C_D^{harm}, and the blue line the median (left out for charn to keep the figure readable). Only *sea* points are used (C_D^{harm} can reach very high values over some lakes in Norway which would distort the picture), and cases with $U_{10} < 4$ m/s are excluded. Below this value C_D^{harm} increases (see Fig. 2.1). The parametrizations are charn ($\alpha = 0.02$), steep, ustar, oost, and zhao36.

16
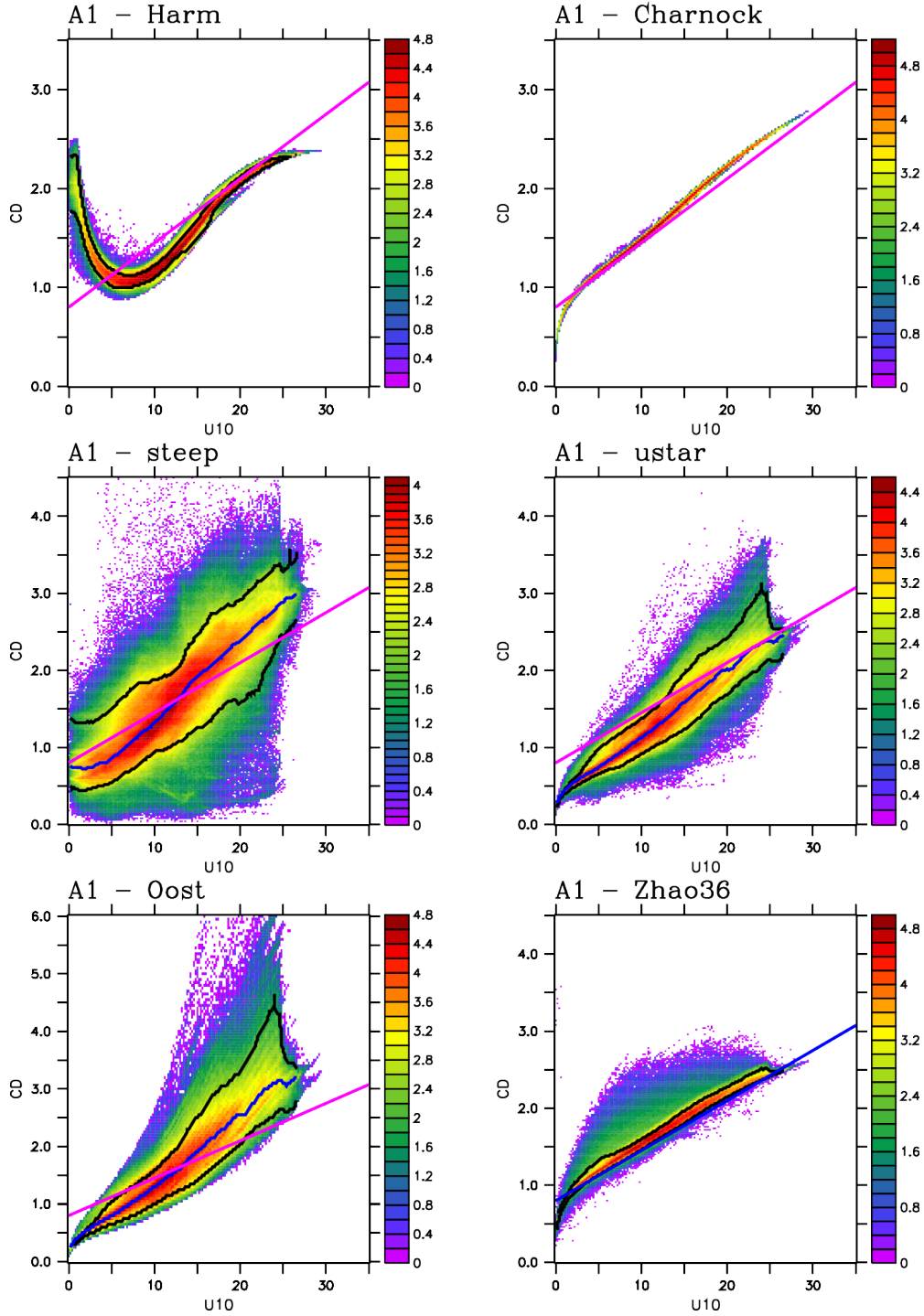
Figure 2.5: Scatter plots (logarithm of the density) of drag coefficients ($10^3 \times C_D$) from different parametrizations against U_{10} for run A1 (Harmonie with ECUME). Only *sea* points are shown. The parametrizations are harm - the parametrization used in Harmonie (ECUME in this case), charn - Charnock relation ($\alpha = 0.02$), steep - steepness based (eq. (1.10)), ustar - wave age based (eq. (1.12), oost - based on the Oost-parametrization (eq. (1.13), and zhao36 - parametrization according to Zhao (eq. (1.16)). The black contour denotes the 95% interval for each value of U_{10} (left out for charn to keep the figure readable), and the blue line denotes the median (left out for harm and charn). As a reference the parametrization of Wu (1982), (eq. (1.8) with $a = 0.8$ and $b = 0.65$, valid for $U_{10} > 6$ m/s) is added (magenta line). It closely follows the Charnock parametrization. Note the different range of the y-axis for oost.
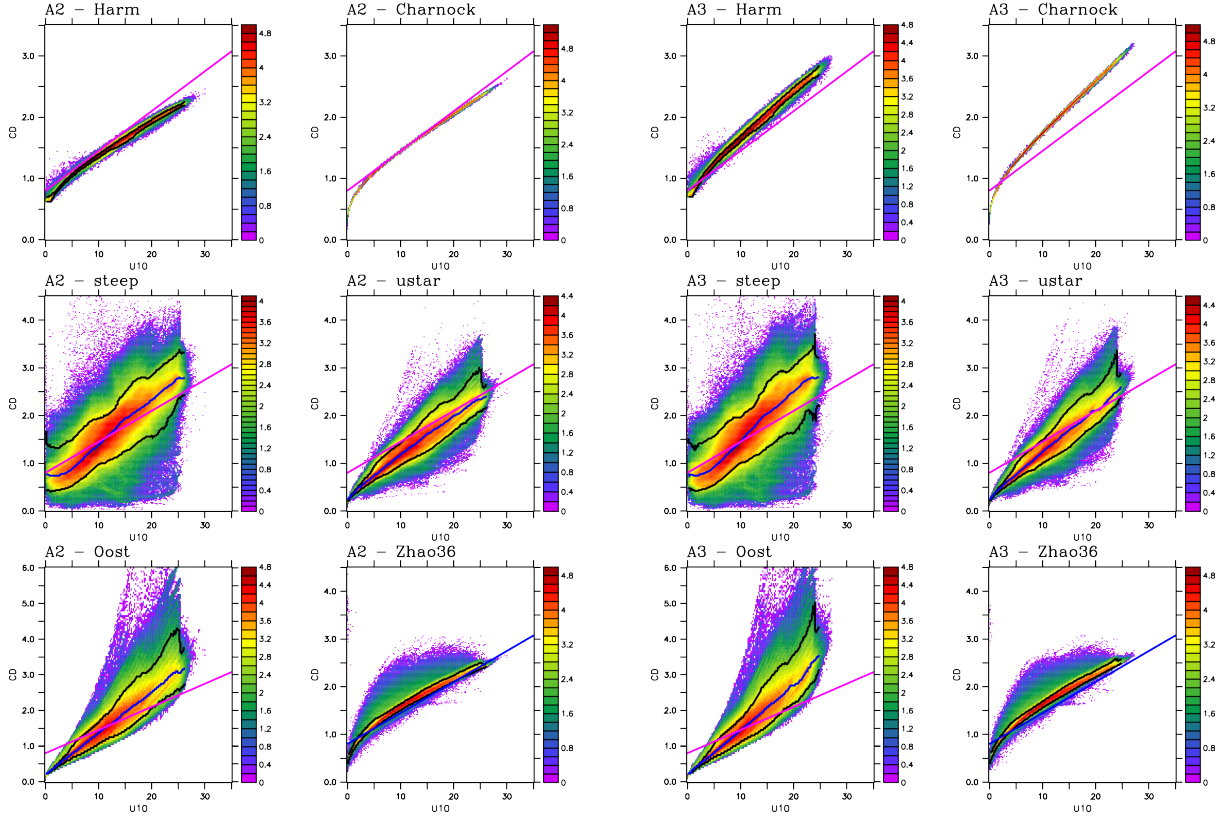
Figure 2.6: As Fig. 2.5, but when Harmonie is run with a Charnock formulation for the drag coefficient. *Left*: $\alpha = 0.015$, *right*: $\alpha = 0.032$.

This can also be understood from Figures 2.5 and 2.6: for ustar and oost, the scatter increases with increasing wind speed.

The correlation patterns for ustar, oost and zhao36 (panels c-e, h-j, m-o) are very similar, with high correlations everywhere. Not surprisingly, the highest correlations are obtained for zhao36. The high correlations for these three parametrizations indicate that their effect could be modelled as a wind speed dependence, and from Figures 2.5 and 2.6 we can infer that the steepness of the $C_D(U_{10})$ relation in Harmonie would need to be increased. Contrary to this, the steep parametrization (panels b, g, l) has relatively low correlations with a distinct spatial pattern, suggesting that it is difficult to incorporate steepness effects into a purely wind dependent parametrization. The low correlations are due to the large scatter and indicate that steepness effects are relatively large, and the fact that a pattern forms, indicates that steepness has a systematic effect on the drag coefficient. Systematic impacts with a spatial pattern have the potential to influence simulated water levels. We investigate this effect in section 2.4.

In Fig. 2.8 we show relative differences between the steepness-based drag coefficients and those generated by Harmonie. The steepness-based drag coefficients can be up to 60% larger than those based on ECUME and the $\alpha = 0.015$ case, and up to 40% larger than those from the $\alpha = 0.032$ case. Note that the latter value for the Charnock parameter has to be considered as high. On the other hand, the steepness-dependent drag coefficients can be lower than those from Harmonie in large regions. A difference of 60% sounds impressive, but in the next section we show that the effects of this large difference are much lower than 60%.

2.3.4 Detailed analysis in one area

We now look into the evolution of some parameters in more detail. We do so for storm B, which reaches its highest wind speeds just west of Denmark. Fig. 2.9 shows time series of U_{10}, H_s, C_D
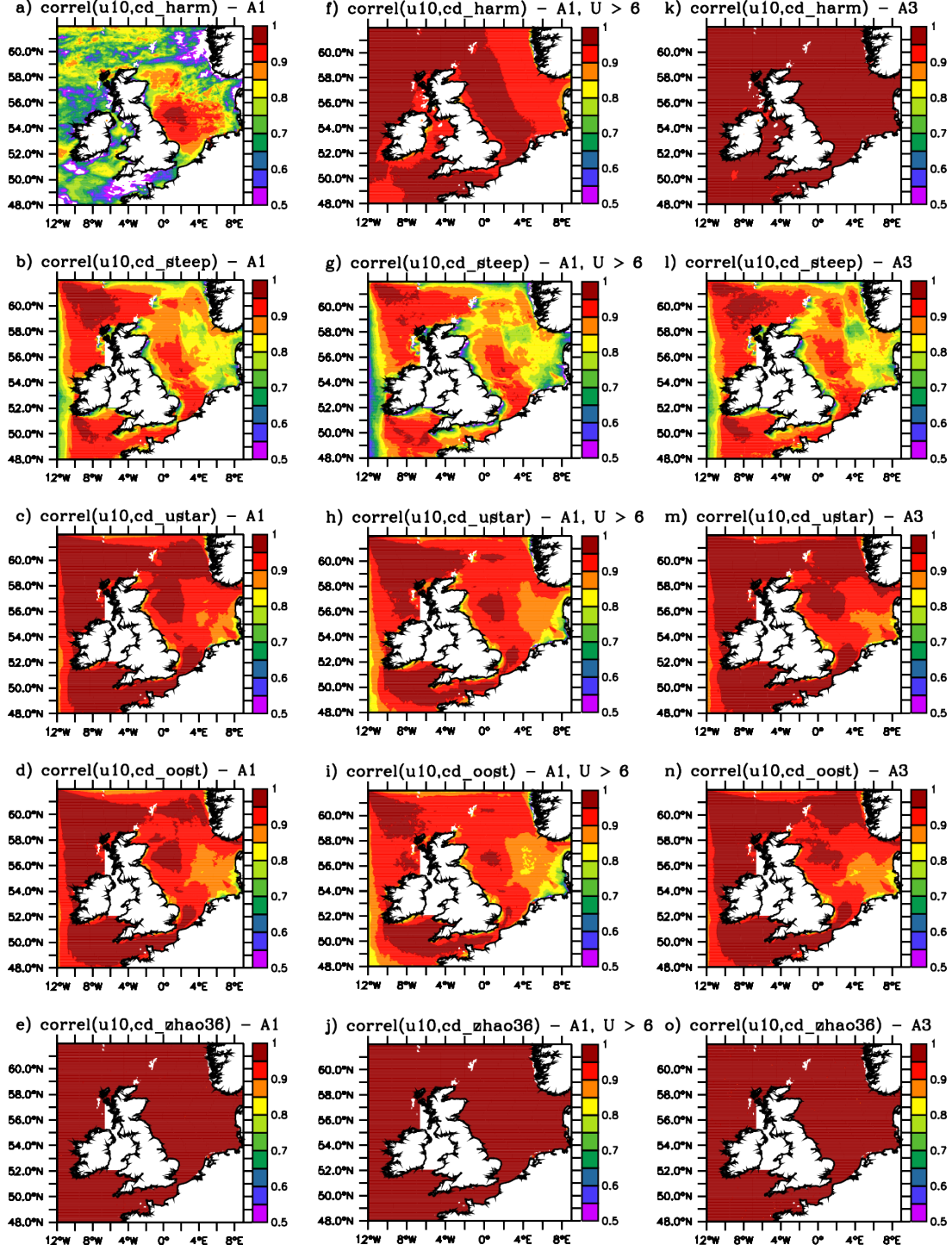
Figure 2.7: Correlation between drag coefficients and wind speed over the whole duration of runs A1 and A3 for different parametrizations. *left column*: A1, all wind speeds; *middle column*: A1, only wind speeds > 6 m/s; *right column*: A3, all wind speeds. The parametrizations used are indicated on the plots.
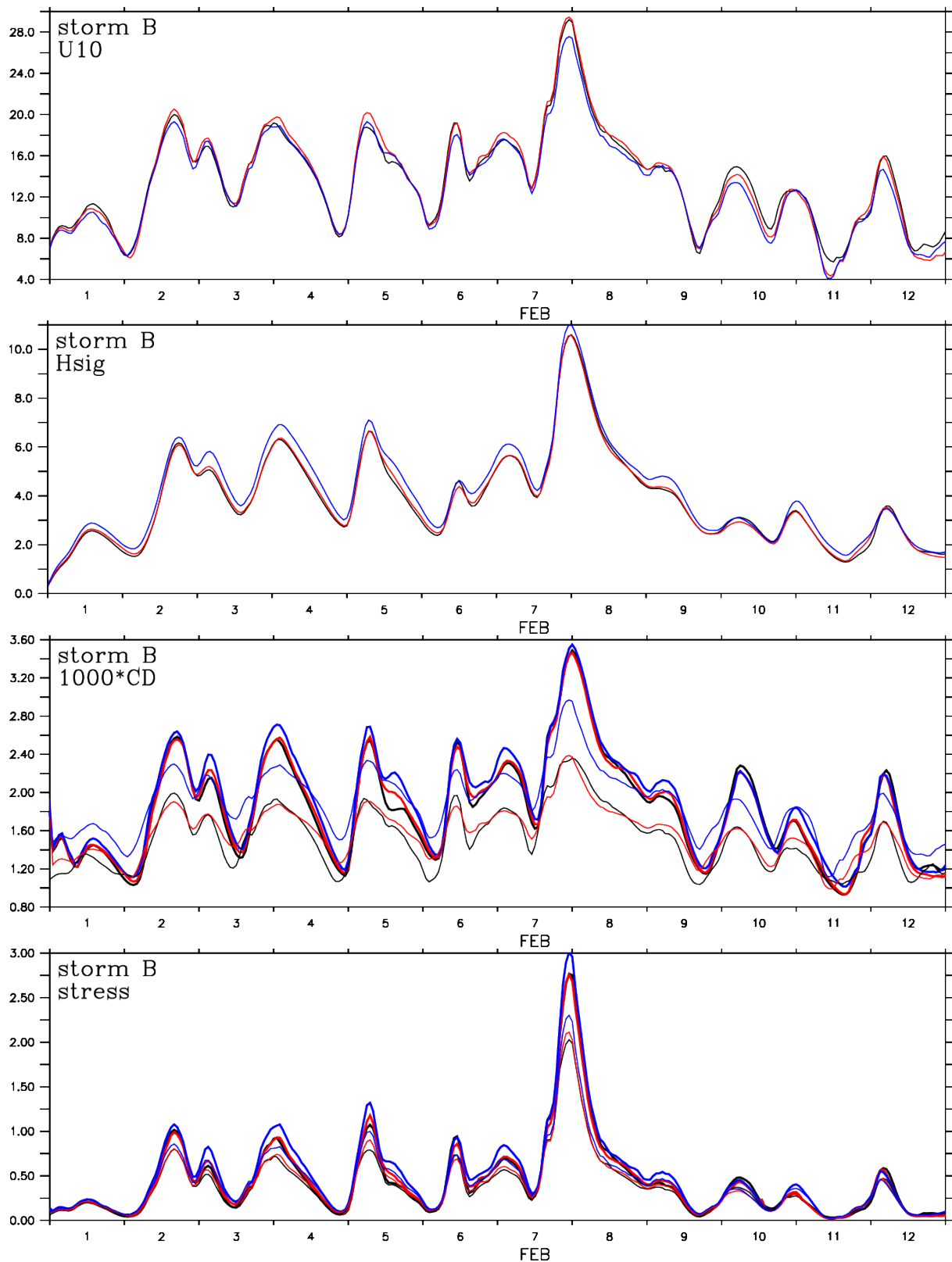
and τ_k averaged over the region $4°E$–$8°E$, $55°N$–$57°N$. The stress is represented by the kinematic stress $\tau_k = u_*^2 = C_D\, U_{10}^2$, i.e., the atmospheric density is not included. We only consider the steepness-based parametrization as it shows the largest differences with respect to the ECUME and the constant-Charnock cases.
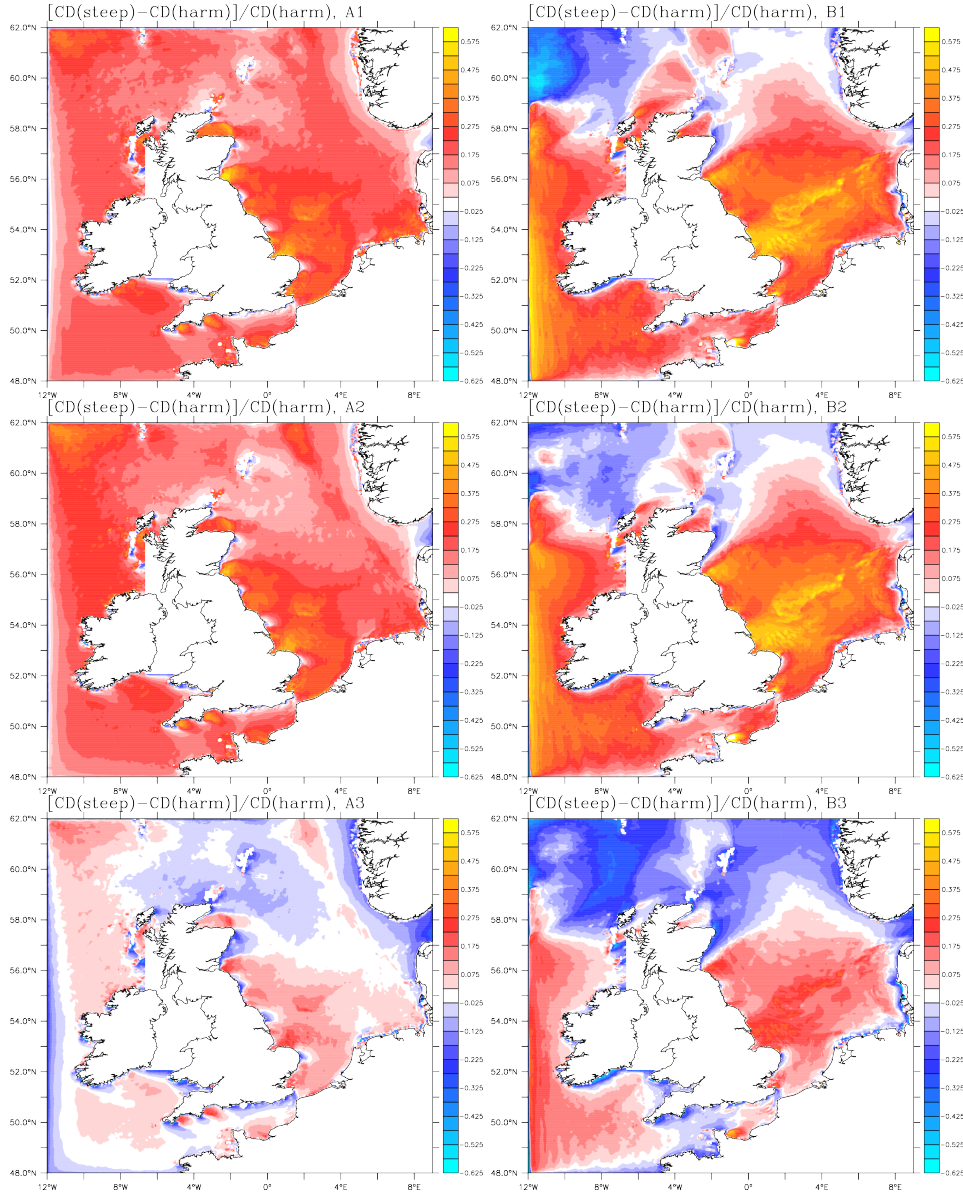
Figure 2.8: Relative difference between the steepness-based drag coefficient and the Harmonie one, $(C_D^{\text{steep}} - C_D^{\text{harm}})/C_D^{\text{harm}}$, averaged over a period of one day around the peak of the storm for runs A1-A3 (left) and B1-B3 (right).

Let us start with the results from Harmonie (thin lines). Although the drag coefficient for the third case ($\alpha = 0.032$) is much larger than for the other two cases, the resulting wind speeds, wave heights and stresses are quite close together, with the higher drag coefficient being compensated by a lower wind speed. The steepness-based parametrization (thick lines) results in drag coefficients that are higher than those from Harmonie most of the time, with only small differences between the three cases, confirming the results from Sect. 2.3.3. The high drag coefficients for the steepness-based parametrizations seem to result in high stress. However, the stress has been calculated using the wind speed from Harmonie, without taking any feedback into account. Thus drag coefficient and wind speed do not correspond to each other. With proper coupling, the higher drag coefficient would reduce the wind speed (compare the wind speeds for the two constant-Charnock cases!) and thus the stress.

Figure 2.9: Time series of U_{10} (m/s), H_s (m), C_D (dimensionless) and τ_k (m^2/s^2) during storm B, averaged over the region where the storm reaches its maximum wind speed (4°E–8°E, 55°N–57°N). Thin lines are for the Harmonie parametrizations with black/red/blue corresponding to parametrizations 1/2/3, respectively, and the thick lines are for the wave steepness based parametrization.
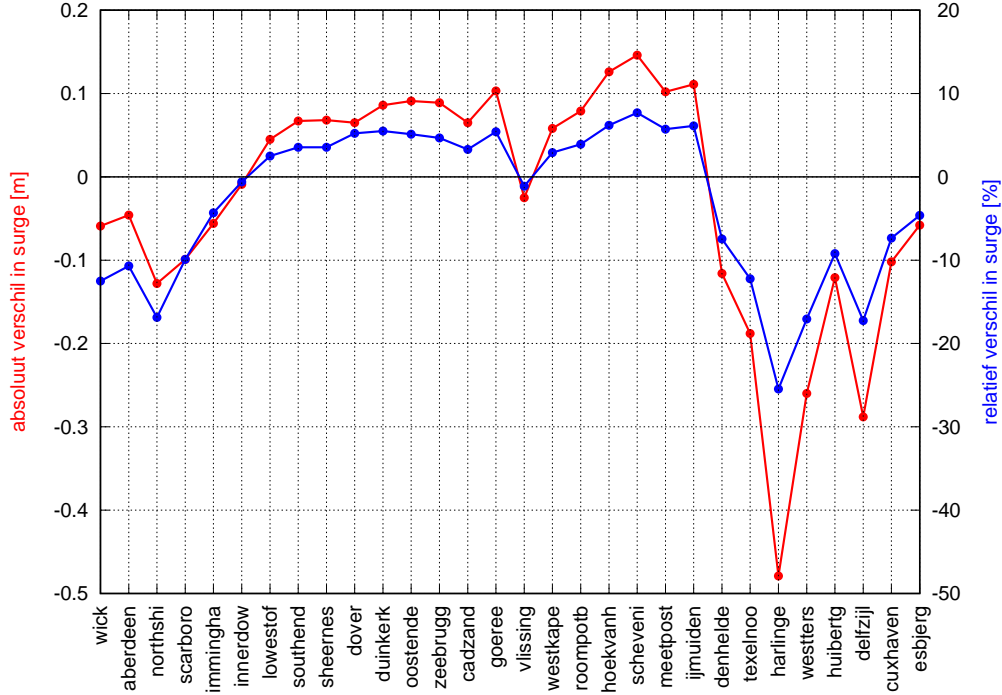
Figure 2.10: Absolute (left-hand axis, red) and relative (right-hand axis, blue) difference of the maximum simulated water levels between a WAQUA run forced with the original Harmonie stress (ECUME parametrization) and a run in which WAQUA was forced by the stress based on wave steepness (storm A). The differences are plotted for stations along the coast of the North Sea, ordered from Scotland (Wick) counterclockwise to Denmark (Esbjerg).

2.4   Effect on water levels

As the dependence of the drag coefficient on wave steepness cannot easily be reproduced as a function of the wind alone, the effect of this parametrization has to be investigated further. The question is whether the altered stress has a large impact on safety-relevant parameters like wave or surge heights. To get a first impression of this impact, we force the WAQUA/DCSMv5 (Gerritsen et al., 1995) storm surge model with and without taking steepness effects into account. In the first run, WAQUA/DCSMv5 is forced by the stress from the Harmonie run A1, i.e., using the ECUME parametrization. In the second run, the forcing is derived from the steepness-based parametrization of the drag coefficient, but keeping the wind as provided by the Harmonie A1 run. Note that neglecting the feedback between the modified drag coefficient and the driving wind leads to stresses that are too high (see Sect. 2.3.4). Both runs are performed without tides.

The differences in maximum simulated water levels between the two runs is displayed in Fig. 2.10. Using the steepness-based parametrisation reduces the water level along the British coast and eastward of IJmuiden, i.e., in the Wadden Sea area, and increases the water level along the south-eastern coast of England and the main part of the Dutch coast. This pattern can be explained by looking at the left panel of Figure 2.11. Along the whole fetch of the wind along the western North Sea, the drag coefficient and thus the stress is higher in the steepness-based parametrization than it is for ECUME, causing higher water levels along the south-western coasts of the North Sea. East of approximately Den Helder, the stress is lower, leading to lower
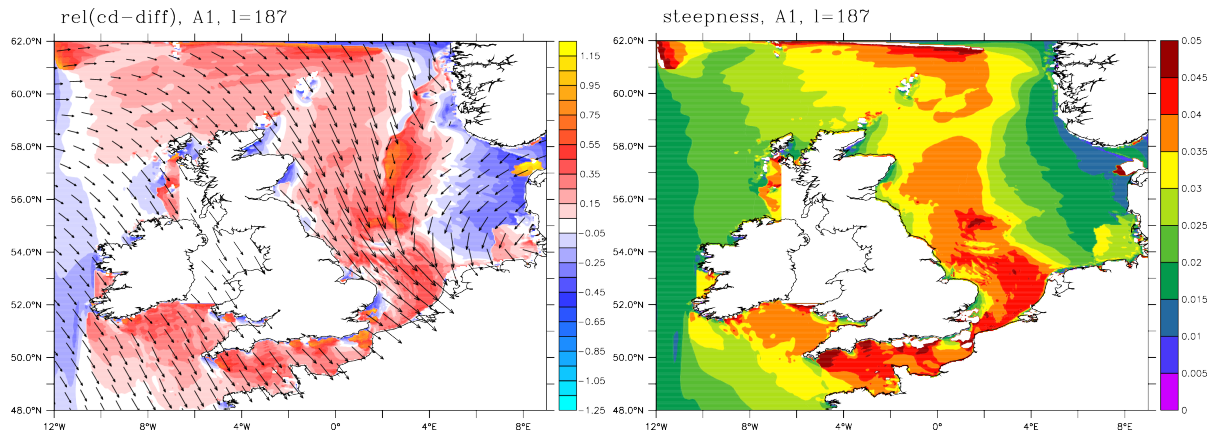
Figure 2.11: *Left*: Relative difference of drag coefficient between steepness-based and ECUME parametrization (colour) and wind direction (arrows) for storm A around the time of the maximum water levels along the coast of the southern North Sea. *Right*: Wave steepness (dimensionless) at the same time.

water levels. The differences in drag coefficient are directly related to the differences in wave steepness across the North Sea (Figure 2.11, right).

Note, however, that the area of higher drag coefficient is also an area of high wind speed, while the area of lower drag coefficient is an area of low wind speed. In a coupled run, where the wind could react to the steepness-based drag changes, the wind speed would decrease in the high-wind speed (high steepness) areas, and increase in the low wind speed (low steepness) ones. This would decrease/increase the stress accordingly and reduce the water level differences displayed in Fig. 2.10. These differences are already small, only a few percent in the areas where the steepness-based drag parametrizations leads to an increase of the modelled water level. Therefore, at least for this one example, it seems not to be important to take the wave dependence of the drag coefficient into account.

2.5   Summary and Conclusions

In this chapter we analyzed the possible effect of waves on the drag coefficient and the ensuing changes in safety-relevant parameters like water levels. Due to the set-up of the experiments performed we can only give tentative answers to these questions. As we only analyzed three storms, using ten-day simulations, our results are not statistically robust. Furthermore, we neglected the (negative) feedback between the modified drag coefficients and the wind speed. The changes we observe are therefore an upper bound for the changes that are to be expected in a coupled setting. For water level the changes observed here are small, not exceeding 8% or 15 cm, and are expected to be even smaller when coupling effects where taken into account.

Three major storms occurring in more than 2400 years of climate model output were downscaled with the high-resolution limited area model Harmonie over the greater North Sea region, and the stress from these downscaling runs has been used to drive the SWAN wave model. The modelled wave parameters were used to calculate wave-dependent drag coefficients according to three different parametrizations found in the literature (see chap. 1). Finally, modified stresses were calculated using the wave-dependent drag coefficients, but without taking the negative feedback between drag coefficient and wind speed into account, and used to drive a surge model.

All wave-dependent parametrizations lead to higher C_D values that grow faster with wind speed, than the wind speed dependent ones used in Harmonie (ECUME and constant-Charnock). This systematic effect could be incorporated in a wind speed dependent parametrization, e.g., by using a higher Charnock parameter. However, in addition to the systematic effect, the wave-

based drag coefficients exhibit a large scatter for a given wind speed. The scatter is largest for the steepness-based parametrization with a width of the 95% interval of roughly ±50%. The scatter is not symmetric. At low (high) wind speeds the steepness-based parametrization is skewed towards positive (negative) deviations from the median, and the other two parametrizations favour positive deviations at high wind speeds. The large asymmetry for the steepness-based parametrization leads to the lowest correlations between C_D and U_{10}. Furthermore, the correlations exhibit a spatial pattern. Both properties suggest that it would be difficult to model the steepness-based effects as a pure wind speed dependence.

In chap. 1 we concluded that the steepness-based parametrisation is the best one to be used in mixed-sea conditions typical for the North Sea. In the present chapter we find that this parametrization leads to the largest effects that presumably cannot be captured by a modification of a pure wind-based parametrization. This underscores that this parametrization is the most relevant to be investigated to asses the importance of coupling effects: it is best suited for the area, and it has the largest impact.

The effect of the modified $C_D(U_{10})$ relation resulting from the steepness-based parametrization on simulated surge levels along the coasts of the North Sea is much smaller than one might expect. For storm A water levels along the Dutch coast increase by less than 8% or 15 cm. This result is reached without taking the feedback between drag coefficient and wind speed into account, which would further reduce the difference. However, this statement is based on only one run and therefore statistically not significant.

The wave-based roughness parametrizations lead to a large scatter in the $C_D(U_{10})$ relation. Its main effect would be to increase the uncertainty of modelled water levels. However, from the results shown here we expect this increase to be small when compared to other modelling uncertainties. As has been shown in Van den Brink (2019), these uncertainties arise from model resolution, both in space and time, and the extrapolation to long return periods.

At first glance our results seem to be at odds with those of Süld et al. (2015), who found that wave-atmosphere coupling results in reduced wave heights and wind speeds and an improved forecast skill. However, they use the wave-induced stress parametrization (1.15) in a fully coupled setting, thereby automatically taking feedback processes into account. Furthermore, they did not look at the stress or the effect of its change on water levels. More work is needed to find out whether their results are really contradicting those reported here.
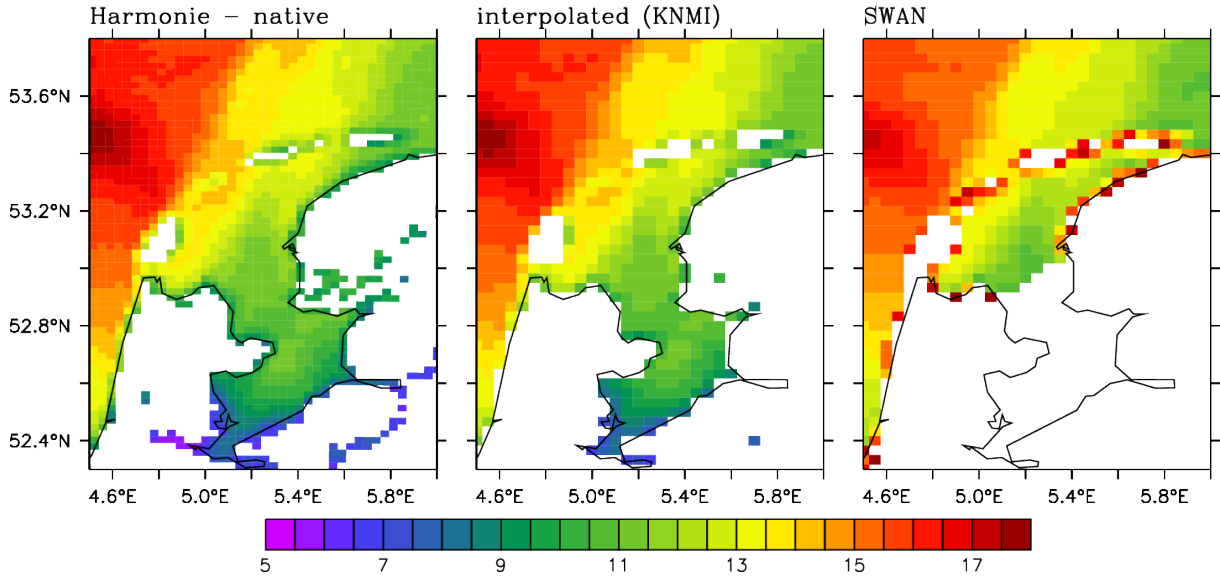
Figure 2.12: Meridional wind field at the native Harmonie resolution, rotated to lat/lon coordinates (*left*), and interpolated to the SWAN grid by KNMI (*middle)* and by Deltares (*right*), for one time step in the area around Lake IJssel. Note that the Harmonie output represents the true wind, while the input to SWAN is the pseudo wind. Therefore, the magnitudes of the two are slightly different.

2.A   Appendix: The SWAN runs

To be consistent, SWAN should be driven by the stress from Harmonie (Van Nieuwkoop et al., 2015). As SWAN cannot use stress directly, the Harmonie stress is first transformed into a pseudo wind based on a Charnock relation (1.4) with $\alpha = 0.0185$, the value used in SWAN. The pseudo wind is then used as input to SWAN.

As explained in Sect. 2.2, Harmonie distinguishes between two kinds of water surface, namely *sea* and *lake*, with different drag parametrizations. Each gridbox contains a certain fraction of both (plus two types of land surface). Most grid points in the SWAN domain are either *sea* or *lake*, and only one value for stress is available. At points containing a mixture of the two (mostly in the Wadden Sea), half the sum of the stress values of the sea and lake tiles is used, with no further weighting. The stress values for both tile types are close together, and details of the weighting appear not to be important.

The pseudo wind fields have been interpolated to the SWAN grid. Figure 2.12 compares a detail of the original Harmonie field of meridional wind, the result of the interpolation by Deltares (as available in their SWAN output), and the field interpolated at KNMI using the Ferret software. Note that the Deltares wind is pseudo wind and therefore differs in magnitude from the true wind. Apart from this difference, there appears to be a large difference in the resulting land-sea mask. It is clear from this figure that the driving wind from Harmonie and the resulting wave information from SWAN may be incompatible in areas affected by this incompatibility (mainly the Wadden Sea), and that the evaluation presented in this report should be treated with caution in that area.

SWAN runs are performed for the greater North Sea domain (e.g., Fig. 2.2) at a horizontal resolution of 0.05° ($\approx$ 5 km), excluding Lake IJssel. For Lake IJssel extra runs with a higher-resolution version have been performed, but they are not analysed here. The runs have been performed using version SWAN 41.20A (`http://swanmodel.sourceforge.net/download/zip/swan4120AB.tar.gz`). Standard parameter settings are applied, water levels are assumed uniform, and currents are not included. The imposed (pseudo)wind is translated into stress using a Charnock relation (1.4) with $\alpha = 0.0185$.

Bibliography

Bengtsson, L., U. Andrae, T. Aspelien, Y. Batrak, J. Calvo, W. de Rooy, E. Gleeson, B. Hansen-Sass, M. Homleid, M. Hortal, K. Ivarsson, G. Lenderink, S. Niemelä, K.P. Nielsen, J. Onvlee, L. Rontu, P. Samuelsson, D.S. Muñoz, A. Subias, S. Tijm, V. Toll, X. Yang, and M.Ø. Køltzow (2017): The HARMONIE–AROME Model Configuration in the ALADIN–HIRLAM NWP System. *Mon. Wea. Rev.*, **145**, 1919–1935, doi: 10.1175/MWR-D-16-0417.1

Bidlot, J.R. (2012): Present status of wave forecasting at E.C.M.W.F. *Workshop on Ocean Waves*, ECMWF, June 25-27, 2012. Presentation available from `https://www.ecmwf.int/sites/default/files/elibrary/2012/14784-present-status-wave-forecasting-ecmwf.pdf`

Bonekamp, H., G.J. Komen, A. Sterl, P.A.E.M. Janssen, P.K. Taylor, and M.J. Yelland (2002): Statistical comparisons of observed and ECMWF modeled open ocean surface drag. *J. Phys. Oceanogr.*, **32**, 1010-1027

Cavaleri, L., S. Abdalla, A. Benetazzo, L. Bertotti, J.R. Bidlot, Ø. Breivik, S. Carniel, R.E. Jensen, J. Portilla-Yandun, W.E. Rogers, A. Roland, A. Sanchez-Arcilla, J.M. Smith, J. Staneva, Y. Toledo, G.Ph. van Vledder, and A.J.van der Westhuysen (2018): Wave modelling in coastal and inner seas. *Progr. Oceanogr.*, **167**, 164-233, doi: 10.1016/j.pocean.2018.03.010

Charnock, H. (1955): Wind stress on a water surface. *Q. J. R. Meteorol. Soc.*, **81**, 639-640

Drennan, W.M., K.K. Kahma, and M.A. Donelan (1999): On momentum flux and velocity spectra over waves. *Boundary-Layer Meteorol.*, **92**, 489-5515, doi: 10.1023/A:1002054820455

Drennan, W.M., H.C. Graber, D. Hauser, and C. Quentin (2003): On the wave age dependence of wind stress over pure wind seas. *J. Geophys. Res.*, **108**, 8062, doi:10.1029/2000JC000715

Drennan, W.M., P.K. Taylor, and M.J. Yelland (2005): Parameterizing the sea surface roughness. *J. Phys. Oceanogr.*, **35**, 835-848

ECMWF (2017): IFS Documentation - Cy43r3 Operational implementation 11 July 2017. PART VII: ECMWF Wave Model. *ECMWF*, Reading, UK. `https://www.ecmwf.int/en/elibrary/17739-part-vii-ecmwf-wave-model` (assessed 4 Dec. 2018)

Gerritsen, H., H. de Vries, and M. Philippart (1995): The Dutch Continental Shelf Model, in: Quantitative Skill Assessment for Coastal Ocean Models, edited by: Lynch, D. and Davies, A., Coastal and Estuarine Studies, 47, AGU, 1995.

Grachev, A.A., and C.W. Fairall (2001): Upward Momentum Transfer in the Marine Boundary Layer. *J. Phys. Oceanogr.*, **31**, 1698-1711, doi: 10.1175/1520-0485(2001)031<1698:UMTITM>2.0.CO;2

Hazeleger, W., X. Wang, C. Severijns, S. Ştefănescu, R. Bintanja, A. Sterl, K. Wyser, T. Semmler, S. Yang, B. van den Hurk, T. van Noije, E. van der Linden, and K. van der Wiel (2012): EC-Earth V2: description and validation of a new seamless Earth system prediction model. *Clim. Dyn.*, **39**, 2611-2629, doi: 10.1007/s00382-011-1228-5

Högström, U., E. Sahlée, A.-S. Smedman, A. Rutgersson, and E. Nilsson (2015): Surface Stress over the ocean in swell-dominated conditions during moderate winds. *J. Atmos. Sci.*, **72**, 4777-4795, doi: 10.1175/JAS-D-15-0139.1

Janssen, P.A.E.M. (1989): Wave-induced stress and the drag of air flow over sea waves. *J. Phys. Oceanogr.*, **19**, 745-754

Janssen, P.A.E.M. (1991): Quasi-linear theory of wind-wave generation applied to wave forecasting. *J. Phys. Oceanogr.*, **21**, 1631-1642

Komen, G.J., L. Cavaleri, M. Donelan, K. Hasselmann, S. Hasselmann, and P.A.E.M. Janssen (1994): Dynamics and modelling of ocean waves. *Cambridge University Press*, Cambridge, UK, 1994

Le Moigne, P. (Ed.) (2018): SURFEX Scientific Documentation, V8.1. `http://www.umr-cnrm.fr/surfex/IMG/pdf/surfex_scidoc_v8.1.pdf`

Oost, W.A., G.J. Komen, C.M.J. Jacobs, and C. van Oort (2002): New evidence for a relation between wind stress and wave age from measurements during ASGAMAGE. *Bound. Lay. Meteor.*, **103**, 409-438

Pineau-Guillou, L., F. Ardhuin, M.-N. Bouin, J.-L. Redelsperger, B. Chapron, J.-R. Bidlot, and Y. Quilfen (2018): Strong winds in a coupled wave–atmosphere model during a North Atlantic storm event: evaluation against observations. *Q. J. R. Meteorol. Soc.*, **144**, 317-332, doi: 10.1002/qj.3205

Rieder, K. F., and J. A. Smith (1998): Removing wave effects from the wind stress vector. *J. Geophys. Res.*, **103**, 1363-1374, doi: 10.1029/97JC02571

Shimura, Tomoya, Nobuhito Mori, Tetsuya Takemi, and Ryo Mizuta (2017): Long-term impacts of ocean wave-dependent roughness on global climate systems. *J. Geophys. Res. Oceans*, **122**, 1995-2011, doi:10.1002/2016JC012621

Smedman, A.-S., X.G. Larsén, U. Högström, K.K. Kahma, and H. Pettersson (2003): Effect of sea state on the momentum exchange over sea during neutral conditions. *J. Geophys. Res.*, **C108**, 3367, doi: 10.1029/2002JC001526

Sterl, A. (2017): Drag at high wind velocities - a review. *Technical Report*, TR-361, KNMI, De Bilt

Stewart, R.H. (2008): Introduction to Physical Oceanography. *Open Textbook Library*, `https://open.umn.edu/opentextbooks/textbooks/introduction-to-physical-oceanography` (accessed 28 Nov. 2018)

Süld, J.K., A. Rasheed, J. Kristiansen, Ø. Sætra, A. Carrasco, and T. Kvamsdal (2015): Mesoscale numerical modelling of met-ocean interactions. *Energy Procedia*, **80**, 433-441, doi: 10.1016/j.egypro.2015.11.447

The SWAN team: SWAN - Scientific and technical documentation SWAN Cycle III version 41.20A. Online documentation (accessed 22 Oct. 2018): `http://swanmodel.sourceforge.net/online_doc/swantech/swantech.html`

Taylor, P.K., and M.J. Yelland (2001): The dependence of sea surface roughness on the height and steepness of the waves. *J. Phys. Oceanogr.*, **31**, 572-590

Tennekes, H. (1973): The logarithmic wind profile. *J. Atmos. Sci.*, **30**, 234-238

Toba, Y. (1972): Local balance in the air-sea boundary process. I. On the growth process of wind waves. *J. Oceanogr. Soc. Jpn.* **28**, 109-120

Tolman, H.L. (2009): User manual and system documentation of WAVEWATCH III^{TM} version 3.14. *Technical Note*, NOAA, `http://polar.ncep.noaa.gov/mmab/papers/tn276/MMAB_276.pdf`

Van den Brink, H. (2019): Het gebruik van de ECMWF seizoensverwachtingen voor het berekenen van de klimatologie van extreme waterstanden langs de Nederlandse kust. *in preparation*

Van der Wiel, K., Wanders, N., Selten, F.M., and Bierkens, M.F.P. (2019): Added value of large ensemble simulations for assessing extreme river discharge in a 2°C warmer world. *Geophys. Res. Lett.*, **46**, 2093-2102, doi: 10.1029/2019GL081967

Van Nieuwkoop, Joana, Peter Baas, Sofia Caires, and Jaco Groeneweg (2015): On the consistency of the drag between air and water in meteorological, hydrodynamic and wave models. *Ocean Dynam.*, **65**, 989-1000, doi: 10.1007/s10236-015-0849-3

Wu, Jin (1982): Wind-stress coefficients over sea surface from breeze to hurricane. *J. Geophys. Res.*, C87, 9704-9706, doi: 10.1029/JC087iC12p09704

Yelland, M., and P.K. Taylor (1996): Wind measurements from the open ocean. *J. Phys. Oceanogr.*, **26**, 541-558.

Zhao, D., and M. Li (2019): Dependence of wind stress across an air-sea interface on wave states. *J. Oceanogr.*, **75**, 207-223, doi: 10.1007/s10872-018-0494-9

Zijlema, M., G.Ph. van Vledder, and L.H. Holthuijsen (2012): Bottom friction and wind drag for wave models. *Coastal Engineering*, 65, 19-26, doi: 10.1016/j.coastaleng.2012.03.002